Comparison of four independently determined structures of human recombinant interleukin-4

Lorna J. Smith[1], Christina Redfield[1], Richard A. G. Smith[2], Christopher M. Dobson[1], G. Marius Clore[3], Angela M. Gronenborn[3], Mark R. Walter[4], Tattanahalli L. Naganbushan[5] and Alexander Wlodawer[6]

[1]Oxford Centre for Molecular Sciences and New Chemistry Laboratory, University of Oxford, South Parks Road, Oxford OX1 3QT UK
[2]SmithKline Beecham Pharmaceuticals, The Pinnacles, Coldharbour Road, Harlow, Essex. UK
[3]Laboratory of Chemical Physics, Building 2, National Institute for Diabetes and Digestive and Kidney Diseases, National Institutes of Health, Bethesda, Maryland 20892 USA
[4]Department of Pharmacology, University of Alabama at Birmingham, UAB station, Birmingham, Alabama 35294, USA
[5]Schering-Plough Research Institute, Bloomfield, New Jersey 07003, USA
[6]Macromolecular Structure Laboratory, NCI-Frederick Cancer Research and Development Center, ABL-Basic Research Program, Frederick, MD 21702, USA

Four independent structures of human interleukin-4, two determined by nuclear magnetic resonance techniques and two by X-ray diffraction, have been compared in detail. The core of this four helix bundle protein is very similar in all the structures but there are some differences in loop regions that are known to be mobile in solution. Careful comparison of the experimental data sets and the methods of analysis of the different laboratories has provided clues to the sources of most of the differences, and also answered some general questions about the accuracy of protein structure determination by these two techniques.

Several protein structures have now been solved by both crystallographic and NMR techniques. This has led to great interest in their comparisons as they provide insights into the similarity between protein structures in the solution and crystalline states, as well as providing a method for identifying errors that may arise from either technique[1]. In general, comparisons have indicated close similarity between structures of proteins in solution and in crystals, particularly in the core[2–4]. However, differences in the quaternary structure of interleukin-8 (refs 5,6) and metal coordination of metallothionein[7,8] have been observed. Attempts have also been made to use data obtained by both techniques to refine a single structure[9]. None of these comparisons has yet involved multiple structures solved independently by both techniques.

An opportunity to make a comparison has arisen in the case of the helical cytokine, human interleukin-4 (IL-4). Here, four independent structures, determined in different laboratories, two by NMR spectroscopy[10,11] and two by X-ray diffraction[12,13], were published within a few months of each other. Prior to these structures, preliminary NMR studies of IL-4 had enabled identification of the correct left-handed four-helix bundle fold for the protein[14,15]. More recently, Powers *et al.* have refined their NMR structure further based on around three times as many experimental NMR restraints as in their previous structure[16].

The comparison of the four high resolution structures of IL-4 has enabled us to investigate the dependence of different regions of the structural models on the exact techniques used in the structure determination as well as the nature of any true differences between IL-4 in solution and in the crystalline state. It therefore provides insights into the interpretation of other comparisons of NMR and X-ray structures. It is particularly interesting to carry out such a comparison for IL-4 as ^{15}N NMR relaxation studies of the protein in solution carried out by Redfield, *et al.*[17] have revealed its intriguing dynamic properties; the two long loops that run the length of the molecule (AB and CD) having a high degree of mobility in solution. This makes attempts to describe adequately the structure of the protein particularly challenging.

Overall comparison of the structures

The four structures of IL-4 are all left-handed four helix bundles with up-up-down-down connectivities (Figs

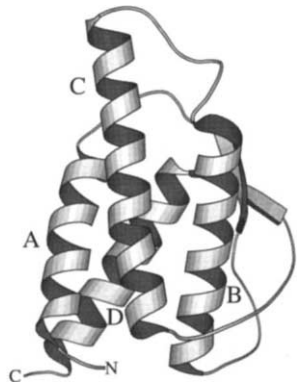

Fig. 1 A schematic diagram showing the four helix bundle fold of human interleukin-4. The diagram was generated using MOLSCRIPT[30].

1,2). A short region of β-sheet connecting the AB and CD loops has also been identified in all the structures. Hence, despite the different techniques and independent approaches used the four research groups, the resulting structures are very similar. In this comparison we concentrate on the details of the structure where differences have been observed.

Helical core

Table 1 gives values of the root-mean-square deviations between the Cα atoms in individual structures. For residues 1–129, the two X-ray structures have an r.m.s.d. of 0.85 Å, while NMR – NMR and NMR – X-ray comparisons reveal r.m.s.ds of 1.9–2.5 Å, the two NMR structures being as different from each other as they are from the X-ray structures. In general, lower r.m.s.ds are observed for the four helices of the protein which represent the core of the structure. The lengths of the helices as quoted by the various research groups differ by up to 5 residues at their amino or carboxy-terminal regions (Table 2). A closer examination shows that these differences arise from the different criteria used to identify the helices rather than from true discrepancies between the structures. Helices can be defined by identifying i to i+4 hydrogen bonds[18] or by recognising residues with local geometries close to those of a regular helix, ϕ −57°, ψ −47° (ref. 19). The first of these methods allows a greater variation in the conformations that can be defined as helical and so gives longer identified helices.

There are slight differences in the packing of helices in the core of the molecule, particularly in the NMR structures. This is revealed in the comparison of the interhelix angles (Table 3). For the Oxford structure it is clear that the orientation of the B helix differs most, especially with respect to the D helix, compared with the other structures, while for the NIH low and high resolution structures the largest differences are in the AC and DA interhelix angles respectively. These differences in interhelix angle do not produce large r.m.s.ds or significant structural differences. Indeed the low backbone r.m.s.d. of the Oxford solution structure from the UAB crystal structure for the A, C and D helices (0.72 Å) indicates that the packing of these helices is little affected by the different B helix orientation. Much of the variation in helix packing can be traced to differences in the NOE data sets of the Oxford and NIH groups (see later).

In all four structures the helices are held together by a core of hydrophobic side chains particularly those of leucine residues. In contrast, the exterior of the protein is highly hydrophilic with many charged side chains, such

Table 1 Pairwise Cα r.m.s.ds between the individual structures of interleukin-4 [1]

	X-ray	NMR		X-ray/NMR			
	NCI UAB	Oxford NIH LR	Oxford NIH HR	NIH HR NIH LR	NCI Oxford	NCI NIH LR	NCI NIH HR
A (4-19)	0.32	1.51	1.46	1.67	0.92	1.57	0.99
B (40-60)	0.32	2.12	1.54	1.49	1.70	1.37	0.82
C (70-94)	0.20	2.03	1.86	0.91	1.28	1.47	1.08
D (109-126)	0.24	2.13	2.64	2.08	1.29	1.57	1.75
AB (20-39)	1.05	2.72	1.68	2.37	1.86	2.54	1.60
BC (61-69)	0.23	1.94	2.28	1.92	2.10	1.59	1.53
CD (95-108)	0.72	2.54	2.59	1.98	2.06	1.77	2.06
(1-129)	0.85	2.47	2.16	2.09	2.18	1.93	1.92
(4-127)	0.53	2.18	2.01	1.84	1.59	1.74	1.45
No outliers[2]	0.29 (121)	1.94 (120)	1.68 (121)	1.58 (120)	1.36 (118)	1.53 (119)	1.15 (119)

NIH LR and NIH HR correspond to the NIH low resolution and high resolution structures respectively.
[1]The r.m.s.d.s of the families of calculated NMR structure around the average structures are:
Oxford[10]: Cα r.m.s.d. for residues 3–127 0.99 ± 0.13 Å
NIH low resolution[11]: backbone r.m.s.d. for residues 3–127 1.02 ± 0.16 Å.
NIH high resolution[16]: backbone r.m.s.d. for residues 4–125 0.44 ± 0.03 Å.
[2]This line represents the best superposition, after removing points which deviate by more than 3 σ from the mean r.m.s.d., and thus excludes the outliers.

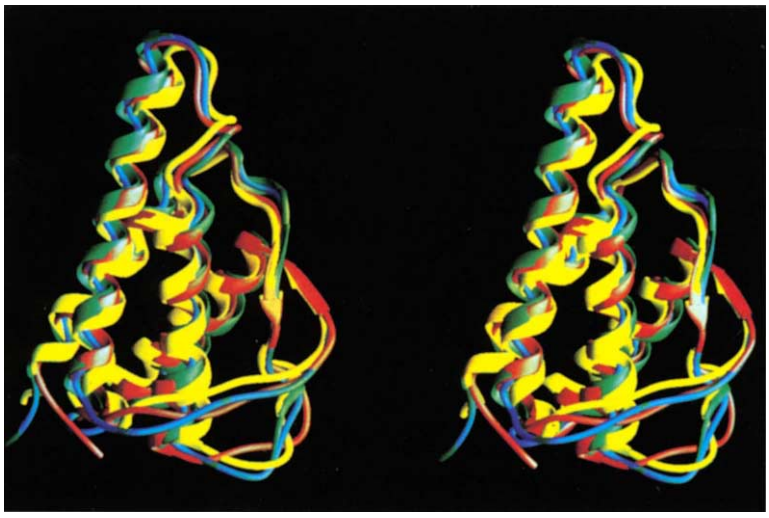

Fig. 2 Stereo diagram showing ribbon traces of the superimposed backbone of the four IL-4 structures. NMR structure from Oxford[10], yellow; high resolution NMR structure from NIH (low resolution structure not shown)[16], green; X-ray structure from NCI[12], blue; X-ray structure from UAB[13], red. The structures are referred to throughout this paper as Oxford, NIH (high and low), NCI and UAB.

Table 2 Regions of identified secondary structure in IL-4[1]

	Helix A	Helix B	Helix C	Helix D	Sheet 1	Sheet 2
Oxford	5–17	41–57	72–90	110–125	28–30	106–108
NIH(low)	5–17	41–60	70–92	109–125	28–30	106–108
NIH(high)	4–20	40–62	69–94	109–124	28–30	106–108
NCI	4–19	40–60	70–94	109–126	27–31	105–109
UAB	5–18	41–55	70–94	109–126	27–31	105–108

[1]These listed in the papers describing the IL-4 structures[10–13, 16].

Table 3 Helix packing

Comparison of interhelix angles (in degrees)

Angle	Oxford	NIH(low)	NIH(high)	NCI	UAB
DA	−144.2	−149.7	−151.4	−146.9	−146.9
BD	−135.8	−143.9	−150.2	−149.5	−150.2
CB	−147.6	−149.4	−155.6	−153.0	−152.2
AC	−159.5	−152.7	−157.5	−158.9	−159.2

Backbone r.m.s.ds (in Å) between the IL-4 structures for the four α helical regions and for sets of three of these helices in turn (The conservative definitions for the helices of residues 5–17, 41–57, 72–90 and 110–125 have been used for these r.m.s.ds).

Structures	ABCD	BCD	ACD	ABD	ABC
UAB/NCI	0.24	0.23	0.22	0.26	0.24
Oxford/NIH(low)	1.71	1.77	1.41	1.73	1.40
Oxford/NIH(high)	1.66	1.77	1.57	1.49	1.23
NIH(low)/NIH(high)	1.27	1.13	1.30	1.32	1.08
Oxford/NCI	1.15	1.24	0.75	1.19	1.06
Oxford/UAB	1.18	1.27	0.72	1.25	1.09
NIH(low)/NCI	1.22	1.17	1.24	1.29	1.01
NIH(low)/UAB	1.20	1.13	1.22	1.27	0.99
NIH(high)/NCI	0.95	0.96	1.08	0.80	0.66
NIH(high)/UAB	0.94	0.94	1.07	0.79	0.70

as those of lysines and arginines, extending out into solution. Many of these charged external side chains are disordered, at least in part, in both the ensembles of NMR structures and are poorly defined by the electron density in the X-ray structures. In the majority of cases these surface side chains are likely to be occupy multiple conformations. The definition of internal side chains is much greater in all the IL-4 structures although, at the current resolution a detailed comparison of their conformations in the individual structures is not warranted. However, the orientations of many of the side chains that define the contacts between the helices are closely similar in the four IL-4 structures. An example of this is shown in Fig. 3.

Loop regions

The largest differences between the structures are found in the loops (particularly AB and CD) and at the N and C termini (Fig. 4). ^{15}N relaxation studies have shown that these regions have high mobility in solution compared with the core of the protein[17]. This mobility could result in disorder in the crystal structures. A strong correlation between the order parameters for the NH vectors and the main chain temperature factors for IL-4 (Fig. 5) suggests that there is at least some degree of disorder in the loops and termini of the crystal structure. The presence of mobility and/or disorder may also lead to ambiguous or insufficient structural data for the regions concerned. These regions will therefore be most depen-

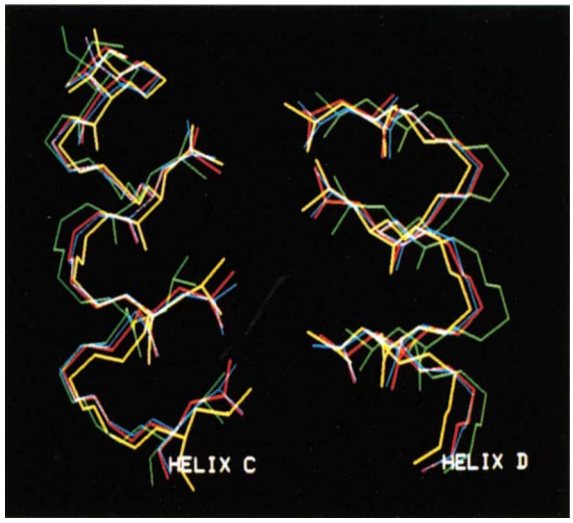

Fig. 3 Local superposition of the four structures of IL-4 showing the leucine side chains involved in contacts between the C and D helices (Leu 79, 83, 86, 90 in helix C, Leu 109, 113, 116 in helix D).

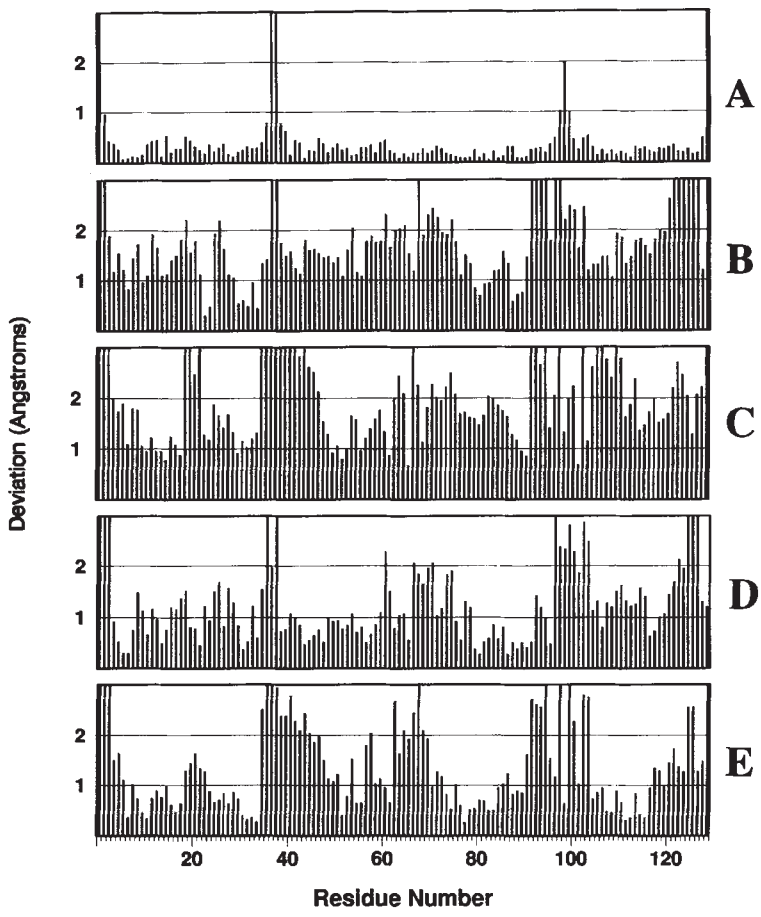

Fig. 4 Selected pairwise comparisons of the Cα deviations between different models of IL-4. Deviations exceeding 3Å are truncated in the plots, in order to preserve a common scale. *a*, NCI and UAB X-ray models. *b*, High resolution NIH and Oxford NMR models. *c*, Low resolution NIH and Oxford NMR models. *d*, NCI X-ray model and NIH NMR high resolution model. e, NCI X-ray model and Oxford NMR model.

Table 4 Final refinement statistics for the X-ray structures of IL-4

Parameters	NCI	UAB
R-factor	21.8%	23.2%
Resolution	10–2.25	6–2.35
No. of Reflections	8085 (83%)	7470 (93%)
No. of Protein Atoms	1048	1048
No. of Waters	33	0
Distance Restraints (Å)		
Bond Distance	0.020 (0.020)	0.022 (0.020)
Angle Distance	0.056 (0.030)	0.047 (0.030)
Planar 1-4 Distance	0.082 (0.050)	0.061 (0.050)
Plane Restraint (Å)	0.016 (0.020)	0.016 (0.020)
Chiral Centre Restraint (Å^3)	0.230 (0.150)	0.222 (0.150)
Non-Bonded Restraints (Å)		
Single Torsion	0.227 (0.300)	0.212 (0.400)
Multiple Torsion	0.305 (0.300)	0.249 (0.400)
Possible Hydrogen Bond	0.231 (0.300)	0.284 (0.400)
Torsion Angle Restraints (Degrees)		
Planar	5.1 (7.5)	2.8 (3.0)
Staggered	25.0 (10.0)	23.0 (15.0)
Orthonormal	37.0 (10.0)	40.8 (20.0)
Isotropic B factor Restraints (Å^2)		
Main Chain Bond	1.468 (1.5)	1.116 (1.0)
Main Chain Angle	3.329 (2.0)	1.843 (1.5)
Side Chain Bond	3.378 (2.0)	1.755 (1.5)
Side Chain Angle	5.539 (3.0)	2.719 (2.0)
Hydrogen Bonds	11.935 (10.0)	—

dent on the precise experimental techniques used. For example, there are differences between the long range NOEs that were unambiguously identified by the Oxford and NIH groups due to the slightly different experimental conditions and the different types of spectra that were analysed in detail by the two groups. The structural properties of these regions will also depend on the interpretation of the available data by the individual research groups. For example, in the NIH low resolution structure dihedral angle restraints were used to define a helical turn for residues 23–25 on the basis of the ^{13}C chemical shift data; this turn was not defined in any of the other structures and hence there is a large r.m.s.d. for this region between the NIH and the other IL-4 structures. Similarly, the greatest difference between the two crystal structures in the AB loop around residues Lys 37 and Asn 38 arises, at least in part, because of different interpretations of the electron density observed for these residues (see later). An additional possibility that cannot be fully discounted, is that one of the conformations populated by the mobile loops in solution may be favoured during crystallization. The high temperature factors for many of the loop residues suggest that this is not a major factor here.

All research groups were able to identify these regions as the 'weak points' of their structures. In the case of the NMR structures, the largest r.m.s.ds across the ensembles of calculated structures were observed for these loop and termini regions, while in the crystal structures the regions had higher B factors and residues were identified which had ϕ and ψ torsion angles in disallowed (or only generously allowed) regions of the Ramachadran plot[20]. These residues are Asn 38 and Thr 40 in the NCI structure, and Lys 37 and Thr 40 in the UAB structure.

Comparison of the X-ray structures

Crystals used to solve the NCI and UAB structures of IL-4 were isomorphous and grown under very similar conditions. The space group was $P4_12_12$, with cell parameters $a = b = 91.8$ Å (both structures), $c = 46.4$ Å (NCI) and 46.2 Å (UAB). The data used for structure refinement were collected on an R-axis image plate at NCI, and with a Siemens X-100A area detector at UAB. The R_{merge} ($R_{merge} = \Sigma_h\Sigma_i |I_{h,i} - \langle I_h \rangle| / \Sigma_h\Sigma_i |I_{h,i}|$)for the NCI data, which contained 9,169 unique reflections (90.7% complete at 2.23 Å) was 6.0%. The UAB intensity data set consisted of 8,531 unique reflections (86,410 observations, 94.9% complete at 2.33 Å) that when merged resulted in an R_{merge} of 9.75%. The NCI and UAB data sets scaled with a mean fractional isomorphous difference (m.f.i.d.) of 14.5% for 7,662 common reflections. When only data with $F > 3\ \sigma\ (F)$ were used in scaling, the resulting m.f.i.d. was 12.2% for 6,849 common re-

flections. These values are very similar to those obtained at NCI for data collected on an image plate and a multiwire detector to slightly lower resolution (A.W., unpublished data). In addition, comparison of the NCI R-axis data with a 2.23 Å intensity data set collected on an R-axis image plate at UAB produced a m.f.i.d. of 12.2% for 8,375 common reflections (M.R.W., unpublished data).

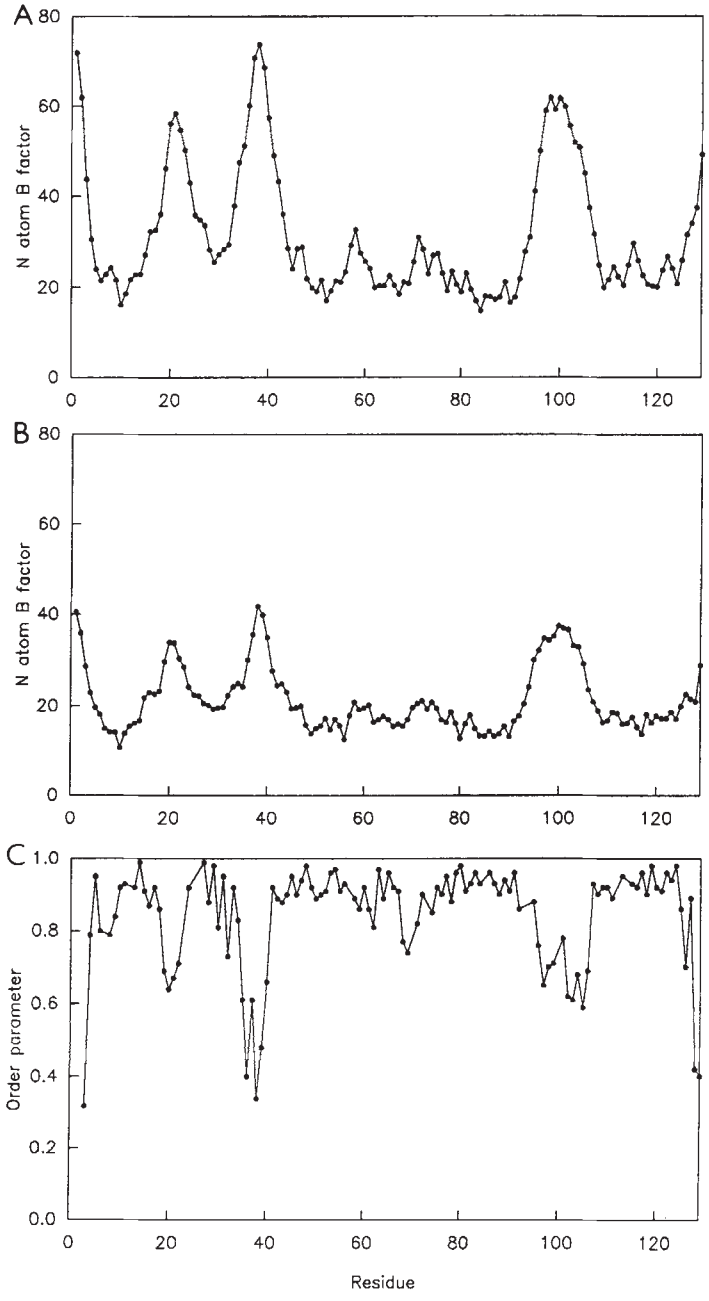

Fig. 5 Comparison of crystallographic temperature factors and solution order parameters for IL-4. *a*, and *b*, show the temperature factors of the main chain nitrogen atoms from the NCI and UAB crystal structures respectively. *c*, shows the order parameters for the ^{1}H-^{15}N vectors in solution (from ref. 17).

Multiple isomorphous replacement phases were obtained from five (NCI) and two (UAB) heavy-atom derivatives. One common site near His 76 was found between the NCI and UAB heavy-atom models. For the NCI structure, interpretation of the weak segments of the electron density map was facilitated by reference to the Oxford structure. All residues in the UAB structure were fitted into MIR and phase combined electron density maps. The NCI structure was refined to an R factor of 0.218 using 8085 reflections with $I > 1.5\ \sigma(I)$ in the resolution range 10–2.25 Å (Table 4). The UAB model was refined with all 7,470 reflections between 6 and 2.35 Å to an R = 0.232.

Both X-ray structures are quite similar, with an r.m.s.d. of 0.29 Å for 121 pairs of Cα atoms (Table 1). The agreement in the highly conserved helical core ranges from 0.20 Å for the C helix to 0.32 Å for A and B helices. For the AB and CD loops, the agreement is poorer (1.05 and 0.72 Å, respectively). The discrepancy for the AB loop can be traced to a difference in assigning the path of the main chain for Lys 37 and Asn 38, where the models used the same density for either the main or side chains, leading to discrepancies of ~3 Å (Fig. 6). In the CD loop, differences of up to 2 Å are caused by a different configuration of the disulphide bridge around Cys 99. In addition, His 1 and Ser 129 were traced very differently in the two structures.

In order to resolve these differences, omit maps were calculated after removing from refinement residues 1 and 129 as well as part or all of the side chains of 25 residues listed in Table 5. The resulting models consisted of 965 atoms and refined to an R = 0.227 for the NCI model and data and 0.221 for the UAB model and data. We also refined the complete NCI model with the UAB data using XPLOR[21] (R = 0.236) and the UAB model with NCI data (R = 0.213).

Careful analysis of the maps resulting from these refinements, in particular the omitmaps described above, showed that both models, while generally similar, had some shortcomings. It appears that residue 1 was traced correctly in the UAB model. The orientation of residue 129 remained unclear, with the UAB tracing more likely. We cannot decide which model describes better the structure for Lys 37 and Asn 38 (Fig. 6), and it is possible that both conformations are present due to interactions in the crystal lattice in this region. It is quite clear that Cys 99 was traced correctly in the UAB model. Of the 25 side chains where the two models differ, it appears that the interpretation was correct for seven side chains each in the NCI and UAB models (Table 5). Neither model described very well the remaining 11 residues; most of these are found on the surface of the protein (nine of them Arg or Lys) and it is likely that some of them are substantially disordered.

Comparison of the NMR structures

Although both the NMR structure determinations used a strategy involving isotopically labelled protein (^{15}N, ^{13}C) and multidimensional heteronuclear NMR experiments, the assignment methods employed by the two groups were very different. The Oxford group used an approach based on the sequential assignment strategy

Table 5 Summary of side chains that differ in the two crystal structures of IL-4

NCI interpretation correct	19, 71, 74, 75, 105, 110, 123
UAB model correct	12, 53, 54, 63, 78, 102, 114
Neither model describes side chain well	2, 5, 21, 32, 42, 61, 81, 115, 117, 121, 126

described by Wüthrich[22], recording seven 3D experiments for both the assignment and structure determination. The NIH group's assignment strategy was based on one-, two- and three-bond heteronuclear J couplings and double and triple resonance experiments[23]. Eleven 3D experiments were recorded for the assignment and a further three to provide the NOE data for the structure calculations (low resolution)[11]. Two 4D experiments, together with several other 3D experiments for the measurement of three-bond coupling constants related to side chain torsion angles, provided additional data for the high resolution structure[16]. Despite different assignment methods the sequential assignments of the two groups are identical. Any slight differences in chemical shift between them can be attributed to the different sample conditions used. Although the NMR data used by the two groups in the structure determinations are broadly similar they are not identical (Tables 6,7). For example, there are 109 and 152 residue pairs between which a long range NOE has been identified in the Oxford and NIH high resolution data sets respectively but an NOE occurs in both data sets for only 89 of these residue pairs. Protein structures were calculated from the Oxford and NIH data using simulated annealing[24,25] and hybrid distance geometry-simulated annealing[26] protocols respectively with XPLOR[21,27].

Table 8 shows the results of a comparison of the Oxford and NIH high resolution structures with the Oxford and NIH data sets. Although the structures exhibit a considerable number of NOE violations from each others' data sets, restrained regularisation of the Oxford and NIH high resolution structures in the presence of the combined NMR data set (all NIH NOEs and dihedral angle restraints + Oxford NOEs) has shown that the majority of the data can be satisfied. (For example, on regularisation the number of NOE violations > 0.5Å falls from 239 to 46 for the Oxford structure and from 133 to 28 for the NIH high resolution structure. The all atom r.m.s.d. between the Oxford structure before and after regularization is 0.87Å and the corresponding value for the NIH structure is 1.10 Å.) The fact that some NOE violations remain does not in itself mean that the data are not all self-consistent (although this possibility is considered further below) since the regularization will only move the structure to a local minimum and not necessarily to the global minimum. The Oxford and NIH structures become more similar on regularization (for residues 4–127 the backbone r.m.s.d. falls from 2.01 to 1.58 Å), the changes involved consisting largely of small shifts in atomic positions. Some larger shifts do, however, occur. At the start of the CD loop the Cα deviation for Leu 93 between the NIH and Oxford structures falls from 3.58 to 1.97 Å, with a reduction from 4.8 to 0.9 Å in the violation of the NIH structure from the NOE between Leu 93 HD1 and Leu 14 HD* in the Oxford data set. In this same region the violation of the Oxford structure from the NOE between Trp 91 HE3 and Cys 46 HA in the NIH data set drops from 5.7 to 0.7 Å. It is important to note that the majority of the initial NOE violations involve side chain atoms rather than the main chain. In many cases the side chains can have different conformations in the two NMR structures without significant differences in the backbone conformation. Indeed, since many of the side chains, particularly those on the surface of the protein, are likely to be mobile in solution, the NOE data may not be compatible with a single conformation of some side chain groups. Regularization also increases the agreement between the NMR and crystal structures although this is not so pronounced (for example, in the NIH structure the backbone r.m.s.d. from the NCI crystal structure for residues 4–127 falls from 1.35 to 1.20 Å while for the Oxford structure the r.m.s.d. falls from 1.61 to 1.49 Å).

Table 6 Summary of the number of NOE, hydrogen bond and dihedral angle restraints in the Oxford and NIH NMR data sets

NOE's	Oxford	NIH low	NIH high
Total	1753[1]	823	2515
Intraresidue	386	0	884
Sequential	557	283	522
1 < li-jl ≤ 5	474	305	549
li-jl > 5	318	235	560
Hydrogen bonds[2]	27	49	51
Torsion angle restraints	101	183	356

[1]1,360 of the NOE's were used in the preliminary calculations that determined the topology and an initial low resolution structure[14].
[2]Number of pairs of hydrogen bond restraints.

Details of the Oxford and NIH data sets

As discussed above the BD interhelix angle in the Oxford structure differs somewhat from that observed in the other structures (despite being well defined in the Oxford ensemble of low-energy structures). This results in a greater deviation of the Oxford structure from the crystal structures in the region of the B helix than the NIH structure (Fig. 4*d*, *e*). The Oxford structure has been found to violate a significant number of interhelix NOEs involving the B helix in the NIH high resolution data set, three of the violations being greater than 3.5 Å (for example the NOE between Phe 45 HZ and Lys 123 HB1 has a violation of 3.8 Å). All these NOEs involve side chain protons only. The Oxford data set itself contains no NOEs between the A and B or between the B and D helices. On regularization there is a shift in the B helix orientation in the Oxford structure (BD angle changes from –135.8° to –137.9°) resulting in a slightly better agreement with the BD interhelix angles observed in the other structures. The sizes of the NOE violations are also reduced although regularisation is not sufficient

Table 7 Comparison of the NOE data sets

Number of residue pairs between which an NOE has been identified

NOE type[1]	Oxford	NIH high	Common to Oxford and NIH[2]
Long range	109	152	89
Medium range	207	184	134

[1]Long range |i-j| > 5; medium range 1 < |i-j| ≤ 5.
[2]Number of residue pairs between which an NOE occurs in both the Oxford and NIH high resolution NMR data sets.

to overcome the barriers required to bring the B helix into its optimal orientation.

NOE violations remain after regularization for both the NIH and Oxford structures around residues 36–38, 103–105, and also in the BC loop. For example, both structures violate several NOEs in these regions by more than 0.5Å (Lys 37 HN – Ala 34 HB#, Gly 67 HN – Ala 68 HN, Ala 68 HB# – Arg 75 HN and Glu 103 HG# – Asx 105 HN). There are also violations in both structures greater than 5° for the dihedral angle ψ restraints of residues 36 and 104 in the NIH data set. It appears that the combined data are not consistent with single conformations in these regions all of which are recognized to be mobile and so may be populating multiple conformations in solution (low order parameters are found for the NH vectors of residues 36–38 and 103–105 and short T_2 values are found for several residues in the BC loop[17]). Residues 38 and 105 are the sites of Asp to Asn mutations in the protein studied at NIH, so a true difference between the structures may exist in these regions. In this regard it is interesting to note that the final part of the CD loop and the start of helix D (residues 105-115) in the Oxford structure has a lower deviation from the NCI crystal structure than the NIH structure (Fig. 4*d*, *e*).

The comparison highlights the problems of using an average structure to represent an ensemble of NMR structures. Where there are disordered regions in NMR structures (due to mobility and/or lack of data) the average torsion angles observed may not be similar to any of those found in an ensemble of NMR structures. This occurs, for example, in the loops in the Oxford structure. For many residues in these loops no angle restraints were included in the structure calculations and so angles covering the whole 360° range of ϕ and ψ are seen in the ensemble of NMR structures. On averaging these, a number of residues have unusual conformations (in disallowed or generously allowed regions of Ramachandran plot) giving poor agreement with the conformations of the other Il-4 structures. For this reason it is important to know the r.m.s.d. distribution for each atom of the family of NMR structures around the mean coordinate position[28]. As with crystallographic B factors, a large r.m.s.d. value will indicate that the coordinate positions are poorly defined by the available experimental data.

Comparison of the crystal structures with the NMR data

In order to assess the consistency of the crystal structures of IL-4 with the NMR data, protons were added to the crystal structure coordinates and the structures were energy minimised using XPLOR[21]. The resulting structures were then compared with the NMR data sets. Both structures violate a considerable number of the NOE restraints in both the Oxford and NIH data sets (Table 9) although, as with the NMR structures, restrained regularisation of the crystal structures with the combined NMR data set removes the majority of the violations with only small shifts in atomic positions (backbone r.m.s.ds between structures before and after regularization are 0.86 and 0.78Å for the NCI and UAB structures respectively). The largest initial NOE violations and consequently the largest changes to the structures on restrained regularisation occur in the AB loop around residues 36–39, the contacts of this region with the start of helix B (Thr 44), the BC loop in the region of residues 60–63, the CD loop around residue 104 and at the C terminus. There are also large NOEs violations involving the aromatic ring protons of Phe 33, Phe 55, Phe 82, Trp 91, Phe 112 and Tyr 124.

The numbers of NOE violations for the crystal structures (prior to regularisation) from the NIH data set are similar to those for the Oxford NMR structure (Tables 8,9). Similarly, the numbers of violations of the crystal structures from the Oxford data set are comparable to those for the NIH high resolution structure. In addition, as for the NMR structures, the largest violations for the crystal structures occur in the regions of highest backbone mobility in solution. Here multiple conformations may be adopted leading to averaged NMR data that may not be compatible with a single conformation.

Restrained regularisation of all the IL-4 structures with the combined Oxford and NIH data set has increased the agreement between the individual structures. For example, the backbone r.m.s.d. for residues 4–127 between the Oxford and NCI structures falls from 1.61 to 1.29 Å, while that between the NIH high resolution and NCI structures falls from 1.35 to 1.05 Å. The agreement between the two X-ray structures is slightly decreased (backbone r.m.s.d. for residues 4–127 increasing from 0.50 to 0.54 Å) reflecting the fact that, in contrast to a joint refinement[9], crystallographic restraints were not included in this regularization.

General discussion

Human IL-4 proved a challenging protein structure to determine both by X-ray diffraction and by NMR spectroscopy. For the X-ray studies, this was partly because of the high mobility of the loop regions which resulted in diffuse electron density and therefore difficulties in tracing the long loop regions. The NMR studies had difficulties partly due to the nature of the overall fold. For helical structures, unlike β-sheet proteins, the long range contacts between regions of secondary structure are overwhelmingly defined by side chain rather than main chain interactions. Both NMR structure determinations therefore had to use double labelled samples of the protein and multidimensional NMR techniques to resolve sufficient side chain-to-side chain NOEs to define adequately the tertiary structure of the protein. It is pleasing that all four independently determined structures of

IL-4 have similar elements of secondary structure and an identical topology, demonstrating the reliability of both NMR and X-ray diffraction techniques and providing considerable confidence in many of the details of the structures.

Detailed comparisons of the Cα r.m.s.ds between the individual structures have shown that the two X-ray structures are very similar to each other (0.53Å r.m.s.d. for residues 4–127). The two NMR structures are also similar, although they differ to a greater extent when compared on this basis (2.01 Å r.m.s.d. for residues 4–127); indeed they are more similar to the X-ray structures than they are to each other. Comparison of the NMR data showed that the sequential assignments of the Oxford and NIH groups are identical although the groups used different assignment procedures. The differences between the NMR structures must therefore arise in part from differences in the data structural collected by the two groups and from their different methods of analysis of the data. However, the r.m.s.d. is a glo-

Table 8 Comparison of the IL-4 NMR structures with the Oxford and NIH high resolution data sets

Number of NOE violations of NIH high resolution structure							
Violation of	0.5–1.0	1.0–2.0	2.0–3.0	3.0–4.0	4.0–5.0	5.0–6.0	6.0 + Å
Oxford data	56	49	18	7	3	0	0
NIH data	0	0	0	0	0	0	0
Number of NOE violations of Oxford structure							
Violation of	0.5–1.0	1.0–2.0	2.0–3.0	3.0–4.0	4.0–5.0	5.0–6.0	6.0 + Å
Oxford data	10	0	0	0	0	0	0
NIH data	93	75	38	12	5	2	4
Comparison of the Oxford and NIH high resolution structures with the NMR data sets after restrained regularization							
Number of NOE violations of NIH structure after regularization							
Violation of	0.5–1.0	1.0–2.0	2.0–3.0	3.0–4.0	4.0–5.0	5.0–6.0	6.0 + Å
Oxford data	26	2	0	0	0	0	0
NIH data	0	0	0	0	0	0	0
Number of NOE violations of Oxford structure after regularization							
Violation of	0.5–1.0	1.0–2.0	2.0–3.0	3.0–4.0	4.0–5.0	5.0–6.0	6.0 + Å
Oxford data	25	3	0	0	0	0	0
NIH data	15	3	0	0	0	0	0

Table 9 Comparison of the IL-4 X-ray structures with the Oxford and NIH high resolution data sets

Number of NOE violations of NCI structure							
Violation of	0.5–1.0	1.0–2.0	2.0–3.0	3.0–4.0	4.0–5.0	5.0–6.0	6.0 + Å
Oxford data	64	44	17	5	2	3	1
NIH data	98	92	26	14	10	2	3
Number of NOE violations of UAB structure							
Violation of	0.5–1.0	1.0–2.0	2.0–3.0	3.0–4.0	4.0–5.0	5.0–6.0	6.0 + Å
Oxford data	69	58	18	7	3	2	0
NIH data	94	118	49	33	10	5	4
Comparison of the IL-4 X-ray structures with the Oxford and NIH high resolution data sets after restrained regularization							
Number of NOE violations of NCI structure after regularization							
Violation of	0.5–1.0	1.0–2.0	2.0–3.0	3.0–4.0	4.0–5.0	5.0–6.0	6.0 + Å
Oxford data	34	7	0	0	0	0	0
NIH data	15	1	0	0	0	0	0
Number of NOE violations of UAB structure after regularization.							
Violation of	0.5–1.0	1.0–2.0	2.0–3.0	3.0–4.0	4.0–5.0	5.0–6.0	6.0 + Å
Oxford data	32	7	0	0	0	0	0
NIH data	11	3	0	0	0	0	0

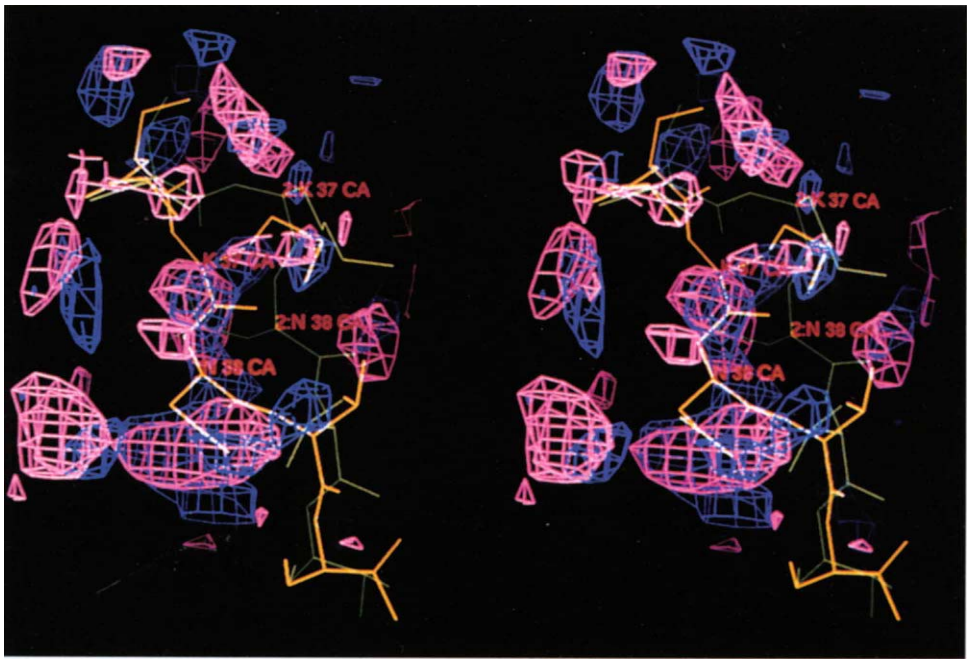

Fig. 6 Stereo diagram showing the difference electron density for residues Lys 37 and Asn 38. F_o-F_c omit electron density maps (contour level 1.5σ) were calculated from phases in which 40 cycles of positional refinement were undertaken in the absence of the two residues to remove model bias. NCI model and electron density are shown in green and pink, respectively, UAB model and electron density are coloured yellow and blue.

bal measure of the similarity between two structures and in many cases the local conformations of residues in the two NMR structures are as similar as in the X-ray structures.

The largest differences between all four structures were found in exposed surface regions, especially those with high mobility. These discrepancies may arise from true differences between the solution and crystal structures, from the different ways in which motion and the presence of multiple conformations will affect the experimental NMR and X-ray diffraction data, and from differences in how the individual research groups interpreted ambiguous or insufficient data. None of the structures able to define these mobile loop regions in IL-4 adequately; a more realistic picture of the conformations adopted in these regions is, however, gained from looking at the range of conformations seen in all four structures than from analysis of any one individual structure.

This comparison highlights the importance of careful analysis of individual protein structures (whether determined by NMR or X-ray diffraction) in order to recognize regions where the observed conformation may be affected by mobility or the precise way in which the experimental data were interpreted or analysed. As structure determinations become more routine and multiple independent structures of other proteins arise, further comparisons of this type should be carried out to produce both a clearer picture of the structure of the proteins concerned and a better understanding of the strengths and weaknesses of NMR and X-ray diffraction techniques in the determination of protein structures.

Methods

The files used in these comparisons were the NMR structure from Oxford[10], both the low and high resolution NMR structures from NIH[11,16] and the X-ray structures from NCI[12] and UAB[13] which have been deposited at the Brookhaven Protein Data Bank as 1ITL, 1BBN, 1ITI, 1RCB, and 2INT respectively. The structures are referred to throughout this paper as Oxford, NIH, NCI and UAB.

All proteins compared in these studies were obtained by recombinant methods and were not glycosylated. In addition to the native sequence (residues 1–129), the Oxford protein had an N-terminal methionine, the sample used at NCI had an N-terminal methionine in about half of the molecules, while the NIH sequence was extended by four residues. These extra residues are not used in the comparisons and the sequence numbers used throughout are those of the native protein (thus the numbers used by Powers *et al.*[16] need to be decreased by four). In addition, IL-4 studied by the NIH group has an Asp to Asn mutation for residues 38 and 105. The NMR work of the Oxford group was carried out at pH 5.6 and 35 °C and at pH 4.5 and 20 °C, while that of the NIH group was performed at pH 5.7 and 36 °C. The X-ray structures of the NCI and UAB groups are for crystals at pH 6.0 and 5.8 respectively.

All coordinates were superimposed on the NCI set using the program ALIGN[29]. Only Cα atoms were used for the alignment and, in addition to superimposing the whole molecule and the individual structural regions, superpositions were made in which the atoms for which significant differences were observed were excluded ('no outliers' in Table 1). The number of atoms used in these superpositions is listed in the bottom line to Table 1.

The program XPLOR[21] was used for the refinements of the NCI structure with the UAB data and the UAB structure with the NCI data, and also in the restrained regularisation of the structures with the combined NMR data set. In the latter the non-bonded interactions were represented solely by a quartic van der Waals' repulsive term[26,27].

Received 9 February; accepted 22 March 1994.

Acknowledgements
Research sponsored in part by the National Cancer Institute, DHHS, under contracts with ABL (A.W.) and by the AIDS targeted Antiviral Program of the Office of the Director of the National Institutes of Health (G.M.C. and A.M.G.). This is in part a contribution from the Oxford Centre for Molecular Sciences which is supported by the U.K. Science and Engineering Research Council and the Medical Research Council. The research of C.M.D. is supported in part by an International Research Scholars Award from the Howard Hughes Medical Institute. L.J.S. is supported by a E. P. Abraham Junior Research Fellowship from St. Cross College, Oxford. The contents of this publication do not necessarily reflect the views or policies of the Department of Health and Human Services, nor does mention of trade names, commercial products, or organisations imply endorsement by the U.S. Government.

1. Billeter, M. Comparison of protein structures determined by NMR in solution and by X-ray diffraction in single crystals. *Q. Rev. Biophys.* **25**, 325–377 (1992).
2. Billeter, M., Kline, A.D., Braun, W., Huber, R. & Wüthrich, K. Comparison of the high-resolution structures of the α-amylase inhibitor tendamistat determined by nuclear magnetic resonance in solution and by X-ray diffraction in single crystals. *J. molec. Biol.* **206**, 677–687 (1989).
3. Clore, G.M. & Gronenborn, A.M. Comparison of the solution nuclear magnetic resonance and X-ray structures of human recombinant interleukin-1β. *J. molec. Biol.* **221**, 47–53 (1991).
4. Berndt, K.D., Güntert, P., Orbons, L.P. M. & Wüthrich, K. Determination of a high-quality nuclear magnetic resonance solution structure of the bovine pancreatic trypsin inhibitor and comparison with three crystal structures. *J. molec. Biol.* **227**, 757–775 (1992).
5. Baldwin, E.T. *et al.* Crystal structure of interleukin-8: symbiosis of NMR and crystallography. *Proc. natn. Acad. Sci. U.S.A.* **88**, 502–506 (1991).
6. Clore, G.M. & Gronenborn, A.M. Comparison of the solution nuclear magnetic resonance and crystal structures of interleukin-8. Possible implications for the mechanism of receptor binding. *J. molec. Biol.* **217**, 611–620 (1991).
7. Furey, W.F. *et al.* Crystal structure of Cd, Zn metallothioneine. *Science* **231**, 704–710 (1986).
8. Schultze, P. *et al.* Conformation of [Cd_7] metallothionein-2 from rat liver in aqueous solution determined by nuclear magnetic resonance spectroscopy. *J. molec. Biol.* **203**, 251–268 (1988).
9. Shaanan, B. *et al.* Combining experimental information from crystal and solution studies: joint X-ray and NMR refinement. *Science*, **257**, 961–964 (1992).
10. Smith, L.J. *et al.* Human interleukin 4: The solution structure of a four-helix bundle protein. *J. molec. Biol.* **224,** 900–904 (1992).
11. Powers, R. *et al.* Three-dimensional solution structure of human interleukin-4 by multidimensional heteronuclear magnetic resonance spectroscopy. *Science* **256,** 1673–1677 (1992).
12. Wlodawer, A., Pavlovsky, A. & Gustchina, A. Crystal structure of human recombinant interleukin-4 at 2.25 Å resolution. *FEBS Lett.* **309**, 59–64 (1992).
13. Walter, M.R. *et al.* Crystal structure of recombinant human interleukin-4. *J. biol. Chem.*. **267**, 20371–20376 (1992).
14. Redfield, C. *et al.* Secondary structure and topology of human interleukin 4 in solution. *Biochemistry* **30**, 11029–11035 (1991).
15. Garrett, D.S. *et al.* Determination of the secondary structure and folding topology of human interleukin-4 using three-dimensional heteronuclear magnetic resonance spectroscopy. *Biochemistry* **31**, 4347–4353 (1992).
16. Powers, R. *et al.* The high-resolution three-dimensional solution structure of human interleukin-4 determined by multi-dimensional heteronuclear magnetic resonance spectroscopy. *Biochemistry* **32**, 6744–6762 (1993).
17. Redfield, C. *et al.* Loop mobility in a four-helix-bundle protein: ^{15}N NMR relaxation measurements on human interleukin-4. *Biochemistry* **31**, 10431–10437 (1992).
18. Kabsch, W. & Sanders, C. Dictionary of protein secondary structure: pattern recognition of hydrogen-bonded and geometrical features. *Biopolymers* **22**, 2577–2637 (1983).
19. Schulz, G.E. & Schirmer, R.H. *Principles of Protein Structure.* (Springer-Verlag, New York, 1979) .
20. Morris, A.L., MacArthur, M.W., Hutchinson, E.G. & Thornton, J.M. Stereochemical quality of protein structure coordinates. *Proteins* **12**, 345–364 (1992).
21. Brünger, A.T. *X-plor version 3.1. A system for X-ray crystallography and NMR* (Yale University Press, 1992).
22. Wüthrich, K. *NMR of Protein and Nucleic Acids* (Wiley, New York, 1986).
23. Powers, R. *et al.* ^{1}H, ^{15}N, ^{13}C and ^{13}CO assignments of human interleukin-4 using three-dimensional double- and triple- resonance heteronuclear magnetic resonance spectroscopy. *Biochemistry* **32,** 4334–4347 (1992).
24. Nilges, M., Kuszewski, J. & Brünger, A.T. Sampling properties of simulated annealing and distance geometry. *Proceedings of the NATO Advanced Research Workshop on Computational Aspects of the Study of Biological Macromolecules by NMR.* (Il Ciocco, Italy, 1991) 451–455 (Plenum Press, New York).
25. Nilges, M., Gronenborn, A.M., Brünger, A.T. & Clore, G.M. Determination of three-dimensional structures of proteins by simulated annealing with interproton distance restraints. Application to crambin, potato carboxypeptidase inhibitor and barley serine proteinase inhibitor 2. *Prot. Engng.* **2**, 27–38 (1988).
26. Nilges, M., Clore, G.M. & Gronenborn, A.M. Determination of three-dimensional structures of proteins from interproton distance data by hybrid distance geometry-dynamical simulated annealing calculations. *FEBS Lett.* **229**, 317–324 (1988).
27. Brünger, A.T., Clore, G.M., Gronenborn, A.M. & Karplus, M. Application of molecular dynamics with interproton distance restraints: application to crambin. *Proc. natn. Acad. Sci. U.S.A.* **83**, 3801–3805 (1986).
28. Clore, G.M. *et al.* The three-dimensional structure of α1-purothionin in solution: combined use of nuclear magnetic resonance, distance geometry and restrained molecular dynamics. *EMBO J.* **5**, 2729–2735 (1986).
29. Satow, Y., Cohen, G.H., Padlan, E.A. & Davies, D.A. Phosphocholine binding immunoglobulin Fab McPC603. An X-ray diffraction study at 2.7 Å. *J. molec. Biol.* **190**, 593–604 (1986).
30. Kraulis, P. MOLSCRIPT: a program to produce both detailed and schematic plots of protein structures. *J. appl. Crystallogr.* **24,** 946–950 (1991).